

# Kinetic Insights into Bridge Cleavage Pathways in Periodic Mesoporous Organosilicas

Zeming Sun Aine Connolly Michael O. Thompson\*

Dr. Z. Sun, A. Connolly, Prof. M. O. Thompson

Materials Science and Engineering, Cornell University, Ithaca, New York 14853, USA

Email Address: mot1@cornell.edu (M.O.T.)

**Keywords:** *Bridge cleavage, Periodic mesoporous organosilicas, Millisecond anneal, Reaction kinetics*

Bridging functionalities in periodic mesoporous organosilicas (PMOs) enable new functionalities for a wide range of applications. Bridge cleavage is frequently observed during anneals required to form porous structures, yet the mechanism of these bridge cleavages has not been completely resolved. Here, we reveal these chemical transformations and their kinetic pathways on sub-millisecond timescales induced by laser heating. By varying anneal times and temperatures, the transformation dynamics of bridge cleavage and structural transformations, and their activation energies, are determined. The structural relaxation time for individual reactions and their effective local heating time are determined and compared, and results directly demonstrate the manipulation of different molecules through kinetic control of the sequence of reactions. By isolating and understanding the earliest stage of structural transformations, this study identifies the kinetic principles for new synthesis and post-processing routes to control individual molecules and reactions in PMOs and other material systems with multi-functionalities.

## 1 Introduction

Periodic mesoporous organosilicas (PMOs), porous silica networks containing organic entities, have attracted tremendous attention both for their well-ordered porous structures with controlled sizes, and for the interactions with molecules, atoms, and ions enabled by tailored bridge structures [1]. Since the discovery of ordered materials [2] and periodic mesoporous organosilicas [3, 4, 5], their distinctive features have found use in a wide variety of applications including catalysis [6, 7], bioengineering and drug delivery [8], low- $k$  dielectrics [9], adsorption/separation of metals and gases [6, 8], ion exchanges [10], and optics [8].

Sol-gel synthesis [11, 12] of organic-inorganic PMOs have been widely investigated to develop a range of functionalities, synthesis routes, and properties [6, 8, 10, 13]. Advances include introducing specific functional bridge components, from simple chain bridges (methyl [14], ethyl [4, 5, 15, 16, 17, 18, 19, 20, 21, 22], and ethene [3, 4, 23, 24, 25]) to more complicated bridges such as benzene [23, 26, 27, 28], thiophene [29, 30], and ring structures [31], as summarized in **Table 1**. The bridge scheme has been further extended to incorporate non-carbon atoms (*e.g.*, S, Al, N) into bridges using either co-condensation [32, 33, 34, 35] or post-grafting [36] methods, and even expanded to non-silica-based mesoporous materials including metal-oxide-based [37] and sulfide-based [38] materials.

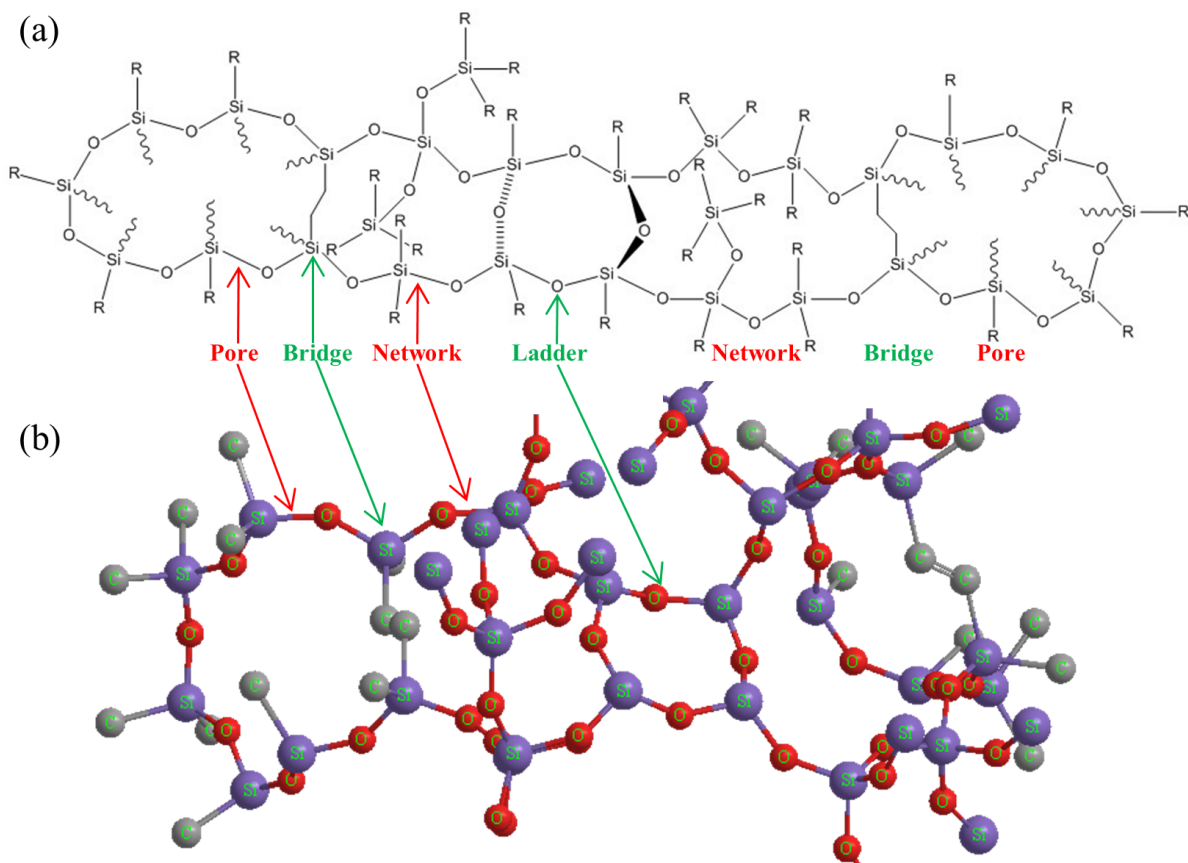


**Figure 1:** (a) 2D chemical structure and (b) 3D projection of ethyl-bridged organosilicas, showing the intrinsic carbon-bridges in addition to pore, network, and ladder motifs.

The functional bridges are of critical interest in PMOs due to the varied functionalities establishing wide-ranging chemical properties [6, 8, 10, 39]. Moreover, additional bridge connections within the framework provide opportunities for tuning mechanical, dielectric, and optical characteristics [8, 40]. Additionally, the integration of these organic bridge motifs can tailor pore structures for surface properties at the nano-scale [21].

However, bridges in PMOs are thermally unstable and may undergo substantial undesirable cleavage during either synthesis or post heat treatment [6, 41]. Several representative bridge-cleavage cases using varied bridge structures, templates, synthesis conditions, and post heat treatments are summarized in Table 1. Factors inducing bridge cleavages include annealing temperatures, acid or base pH levels, extraction steps, processing environment, functionality sizes, and pore sizes.

During synthesis, control of pH is critical to minimize bridge cleavage. The multiple-hour stirring and aging under controlled pH conditions allow hydrolysis and condensation reactions to occur in a transient state without affecting bridge components, resulting in minimal bridge cleavage for synthesis temperatures below 100 °C [18, 24, 32]. Complicated and large bridges, however, are challenging to stabilize in the typically used strong acid or base conditions [42].

Once the framework is established during synthesis, two approaches are commonly

exploited to remove templates (*i.e.*, porogens) and create porous structures. Low-temperature chemical extraction is able to avoid loss of bridge moieties inside the framework [16, 17, 18, 19, 22, 24, 26, 27, 28], while the calcination approach, a post heat treatment for mesoporous silica class materials [22], is challenging [16, 19, 23, 28]. Thermal gravimetric analyses (TGA) show that it is difficult to protect organic bridges even at moderate calcination temperatures (200–350 °C) for minute time frames. At

**Table 1:** Carbon-bridges cleavage conditions for periodic mesoporous organosilicas.

Bridges (Pre-cursors)	Templates	Sol-gel synthesis	Post heat treatment	Bridge cleavage	Ref.
Si-CH <sub>2</sub> -Si (BTEM <sup>a</sup> )	CTAB, CTAC	Aging (25 °C, 96 h)	400–700 °C, 4 h, in air	Onset at 400 °C; completion at 600 °C in air	[14]
Si-CH <sub>2</sub> CH <sub>2</sub> -Si (BTME <sup>b</sup> or BTEE <sup>c</sup> )	CTAB, CTAC, OTAC	Multiple stirring (25 °C, > 24 h), aging (95 °C, 21 h) + extraction (50 °C, 6 h)	TGA	400 °C in nitrogen; 300 °C in air	[5]
	C <sub>n</sub> TMACl	Multiple stirring (25 °C, > 24 h), aging (95 °C, 21 h) + extraction (50 °C, 6 h)	TGA	540 °C in nitrogen; 280 °C in air	[16]
	Brij 76, Brij 30	Stirring (50 °C and 25 °C, > 18 h), aging (95 °C, 24 h) + extraction (50 °C, 8 h)	TGA	400 °C in nitrogen; 338 °C in air	[17]
	P123	Stirring (35 °C, 24 h), aging (85 °C, 24 h) + extraction (25 °C, 10 h)	50–800 °C, 17 h, in air	175 °C in air	[19]
	—	—	35–300 °C, in air	200–300 °C in air	[20]
Si-CH=CH-Si (BTEENE <sup>d</sup> )	PEO-PLGA-PEO	Stirring (25 °C, 0.5 h), aging (100 °C, 24 h) + extraction (25 °C)	500 °C, 10 h, in nitrogen	500 °C in nitrogen	[22]
	CTAB	Aging (25 °C, 96 h)	40–400 °C, 6 h, in air	Onset at 350 °C; completion at 400 °C in air	[3]
	Brij 76	Stirring (50 °C, 12 h), aging (90 °C, 24 h) + extraction (25 °C)	200–1000 °C, 4 h, in air	200–350 °C in air	[23]
	P123	Stirring (40 °C, 24 h), aging (100 °C, 24 h) + extraction	40–400 °C, in air	320 °C in air	[25]
	OTAC	Aging (95 °C, 20 h)	TGA	500 °C in air or nitrogen	[26]
Si-C <sub>6</sub> H <sub>4</sub> -Si (BTEB <sup>e</sup> )	C <sub>n</sub> TMACl	Stirring (25 °C, 24 h), aging (92 °C, 24 h) + extraction (60 °C, 6 h)	TGA	500 °C in air or nitrogen	[27]
	Brij 76	Stirring (50 °C, 12 h), aging (90 °C, 24 h) + extraction (25 °C)	200–1000 °C, 4 h, in air	600 °C in air	[23]
	P123	Stirring (39 °C, 20 h), aging (100 °C, 24 h) + extraction (100 °C, 72 h)	250 °C, in air; TGA	550 °C in air	[28]
	P123	Stirring (40 °C, 20 h), aging (100 °C, 24 h) + extraction (25 °C, 6 h)	TGA	400 °C in air	[29]
Si-C <sub>4</sub> H <sub>4</sub> S-Si (BTET <sup>f</sup> )	PEO-PLGE-PEO	Stirring (40 °C, 24 h), different acidity, aging (100 °C, 24 h) + extraction (56 °C, 24 h)	TGA	300–450 °C in mixed air and nitrogen	[30]
Carbon rings ([ (EtO) <sub>2</sub> -SiCH <sub>2</sub> ] <sub>3</sub> )	CTAB	Stirring (20 °C, 24 h, aging (80 °C, 24 h) + extraction with stirring (25 °C, 48 h)	300–700 °C, in nitrogen	400 °C in nitrogen	[31]
Block copolymers	PEO-PLGA-PEO	Stirring (25 °C, 3 h and 40 °C, 1 h), aging (95 °C, 24 h) + extraction (25 °C, 2 h), stirring (95 °C, 5 h), drying (100 °C, 24 h)	TGA	400 °C in air	[33]
Heteroatom cocondensation [N–, S–] [Al–] isopropoxide	CTAC	Stirring (25 °C, > 12 h), drying (60 °C, 12 h) + extraction (25 °C, 6 h), drying (60 °C, 10 h under vacuum)	TGA	300 °C (no extraction); 200 °C (after extraction)	[34]
	CTAB	Stirring (25 °C, 20 h), aging (100 °C, 24 h) + extraction (25 °C, 6 h)	TGA	300 °C in air	[35]

<sup>a</sup>Bis(triethoxysilyl)methane; <sup>b</sup>Bis(trimethoxysilyl)ethane; <sup>c</sup>Bis(triethoxysilyl)ethane;

<sup>d</sup>Bis(triethoxysilyl)ethylene; <sup>e</sup>Bis(triethoxysilyl)benzene; <sup>f</sup>Bis-(triethoxysilyl)thiophene.

higher temperatures ( $> 400\text{ }^{\circ}\text{C}$ ), the thermal stability of these materials is a significant issue.

After synthesis, PMOs must also tolerate processing conditions required for many electronic devices and other applications, *i.e.*, heating to temperatures above  $400\text{ }^{\circ}\text{C}$  [6, 43]. Consequently, although extraction approaches may initially remove templates without compromising bridges, these bridges may not survive subsequent processing [4, 34]. In most cases, the bridges must be preserved for their functionalities, while some applications may benefit from the generation of terminal dangling bonds of broken bridges [9, 13, 14, 31].

To pursue either of the goals, understanding the underlying kinetics of bridge cleavages is critical and the focus of this work. By determining activation energies and transformation kinetics of each inorganic/organic motif, this work provides guidance to develop heat treatments for PMOs which would facilitate their transition to widespread applications. This work also potentially provides alternative thermal routes to replace the current pH-dependent synthesis protocols that are time-consuming, relatively unstable, and difficult for large bridge structures.

In literature (Table 1), the onset of bridge cleavage is reported to start between  $200\text{ }^{\circ}\text{C}$  and  $600\text{ }^{\circ}\text{C}$  in the air; the variations may be related to variation in processing atmosphere, bridge type, and template type [6]. Several researchers report thermal stability increases by  $60\text{--}260\text{ }^{\circ}\text{C}$  heating in nitrogen rather than air [5, 16, 17], while other researchers report no significant changes with atmosphere [26, 27]. Reduced temperature stability in the air may be a result of reactions between oxygen and carbon bridges [6, 16, 19, 29, 34]. However, water generated by ongoing condensation during post heat treatment [44] may be another source for bridge attacks together with possible nitrogen reactions [16, 17, 34]; this behavior could explain the lack of significant ambient effects. Some research even suggests the onset temperature for bridge cleavages in nitrogen is lower than in air [23, 28]. Although the influence of the ambient gas is not fully clear, we conclude, with caution, that heating ambients are a secondary effect influencing bridge cleavage, with temperature dynamics, as investigated in this work being the primary influence.

The specific chemical structure of the bridge and template components may affect the overall behavior. For example, benzene bridges show slightly higher bridge-cleavage temperatures than other bridges (Table 1). Templates primarily impact the pore size rather than bridge stability; in ethyl-bridged materials, CTAB ( $\sim 2\text{ nm}$  pore), Brij-76 ( $\sim 5\text{ nm}$  pore), P123 ( $\sim 15\text{ nm}$  pore), and PEO-PLGA-PEO (thicker pore wall) templates show similar cleavage temperatures at  $\sim 300\text{ }^{\circ}\text{C}$  in air. In this work, we focus on the Brij-76 template which yields medium-size pores, and ethyl-bridged organosilicas (**Figure 1**). This combination has been widely used to make PMO products (Table 1),

and the general behavioral characteristics can be extended for use in a wide variety of block [32, 33, 34, 35] and graft [36] copolymers.

Studies of thermal decomposition are generally based on either TGA (weight loss as a function of temperature) [3, 5, 14, 15, 16, 17, 20, 23, 25, 26, 27, 28, 29, 30, 31, 33, 34, 35], or chemical characterization of bonding changes after thermal cycling (NMR [3, 4, 5, 14, 15, 25, 26, 30, 31, 33, 35], FTIR [4, 19, 20, 26, 34], and Raman [3, 29, 35]). In this work, we exploit the lateral gradient (single-stripe) laser spike annealing (lgLSA) technique [45] to quantify chemical transformation (bridge cleavage, fully networked framework formation, and template removal) following much shorter timescale sub-millisecond heating. By studying the structural development as a function of the heating duration and peak anneal temperature in this range, we probe the structural transformations and bridge cleavages kinetics, and determine individual reaction activation enthalpies. By understanding the sequence of reactions and their rates, this study identifies new synthesis and/or post-processing routes to control the framework and pore formation while minimizing bridge cleavage.

## 2 Results and Discussion

### 2.1 Transformation dynamics

FTIR spectra were collected as a function of the peak anneal temperature (up to  $\sim 1400^\circ\text{C}$  for heating dwells from 0.5 to 3 ms. **Figure 2a** compares FTIR data from a sample exposed only to ambient conditions ( $400^\circ\text{C}$  sample chuck temperature) to one annealed to  $\sim 1400^\circ\text{C}$  for 3 ms. Detailed data for all conditions (LSA peak temperatures from  $400^\circ\text{C}$  to  $\sim 1400^\circ\text{C}$ ; heating dwells of 0.5, 1, 1.5, and 3 ms) are included in Figure S1. The fully networked Si-O framework formation, carbon-bridge cleavage, and template removal were characterized. The Si-O FTIR peaks include the fully networked framework at  $1072\text{ cm}^{-1}$ , sub-oxide  $\text{SiO}_x\text{C}_y$  at  $1035\text{ cm}^{-1}$ , and the ladder-like structure at  $1105\text{ cm}^{-1}$ . The carbon-bridge cleavage was determined by the change of the Si-CH<sub>2</sub>-CH<sub>2</sub>-Si bridge peak at  $1162\text{ cm}^{-1}$  and a newly appearing Si-CH<sub>2</sub>CH<sub>3</sub> ethyl chain peak at  $1220\text{ cm}^{-1}$ . Changes in the template species were determined from the CH<sub>x</sub> ( $2860\text{--}2920\text{ cm}^{-1}$ ) and CH<sub>3</sub>+ ( $1275\text{ cm}^{-1}$ ) organic complexes [40]. These sub-peaks were fit as Gaussians (Figure 2b,c), with integrated areas calculated for quantification.

The temperature-dependent structural transformations as a function of the laser dwell are presented in Figure S2 and S4. The transformation fraction follows the typical sigmoidal behavior with three temperature regimes: (1) an incubation range with minimal transformation; (2) an intermediate range with rapidly increasing transformation fraction, and (3) a saturation regime where the fraction approaches asymptotically 100% conversion. Depending on the structure’s thermal stability, the temperature ranges of these stages will vary.

With increasing temperature, fully networked frameworks (Figure S2a) form from organic sub-oxides (Figure S2b). In contrast, the intensity of the ladder-like structure (Figure S2c) remains constant with temperature and is not analyzed further. To minimize influences from slight differences in the initial concentrations, a transformation ratio was calculated as  $\text{Ratio} = (\text{Loss or gain}) / \text{Total}$ . The fully networked framework formation (**Figure 3a**) and sub-oxide removal (Figure 3b) exhibit similar transformation ratios with temperature and time.

In contrast, a significant fraction of carbon bridges ( $\text{Si-C}_2\text{H}_4\text{-Si}$  peak) remain intact even at the highest temperature and dwell studied (Figure 3c), with the onset of bridge loss shifting to higher temperatures for shorter dwells. For the 0.5 ms dwell, the bridge peak exhibits minimal changes.

The bridge cleavage can also be quantified by the rise of the  $\text{Si-CH}_2\text{CH}_3$  peak (Figure S4b); the fully cleaved intensity was estimated by a long-duration hotplate anneal [40]. The  $\text{Si-C}_2\text{H}_5$  data (Figure 3d) is consistent with the bridge loss data (Figure 3c),

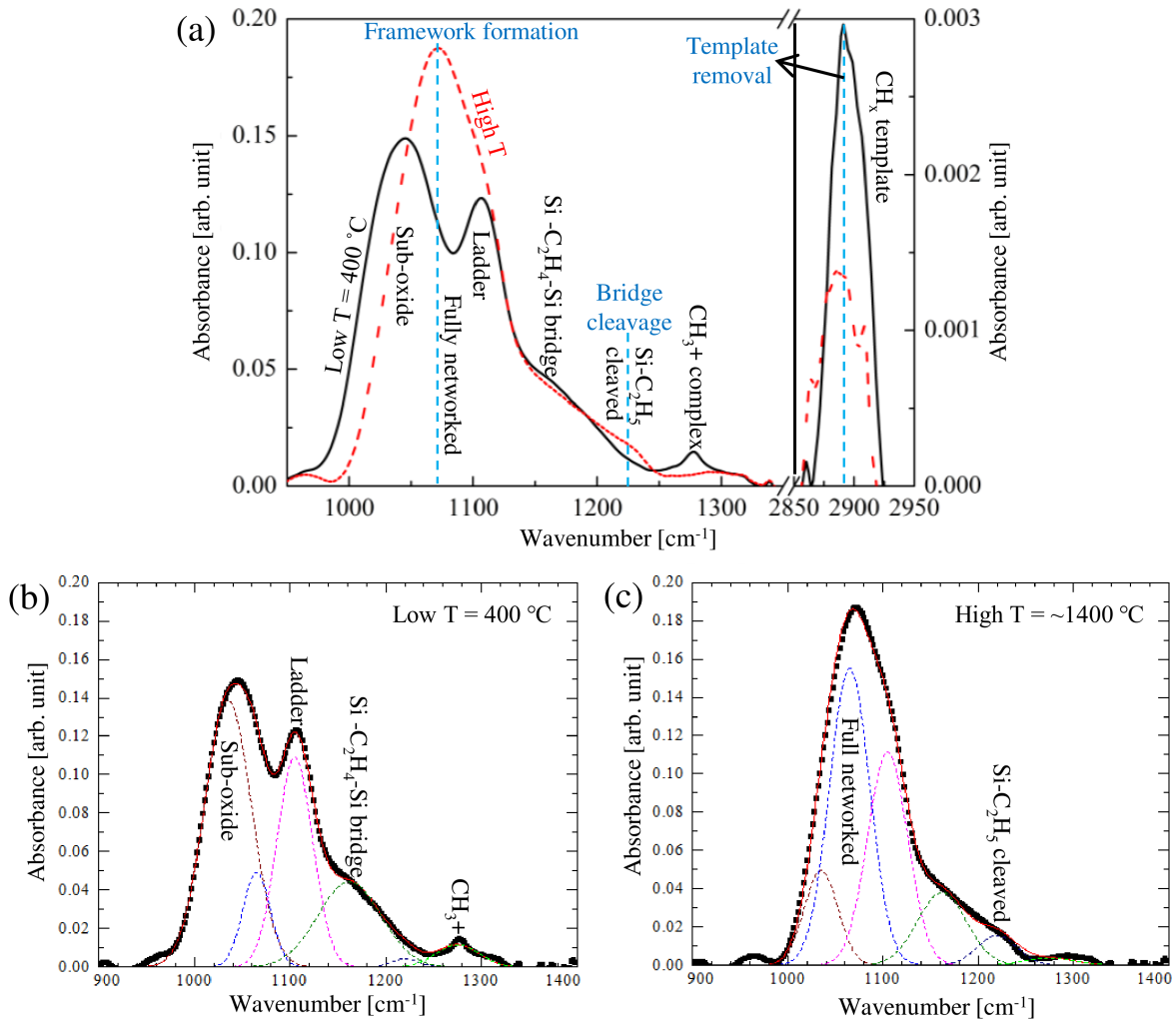


**Figure 2:** (a) Comparison of FTIR spectra after ambient heating to 400 °C (“low T”) and to ~1400 °C (“high T”) for 3 ms. (b,c) Gaussian peak fits showing sub-oxide, fully networked, ladder structures,  $\text{Si-C}_2\text{H}_4\text{-Si}$  bridge,  $\text{Si-C}_2\text{H}_5$  bridge cleavage, and  $[\text{CH}_3+]$  motifs at 400 °C (b) and ~1400 °C (c).

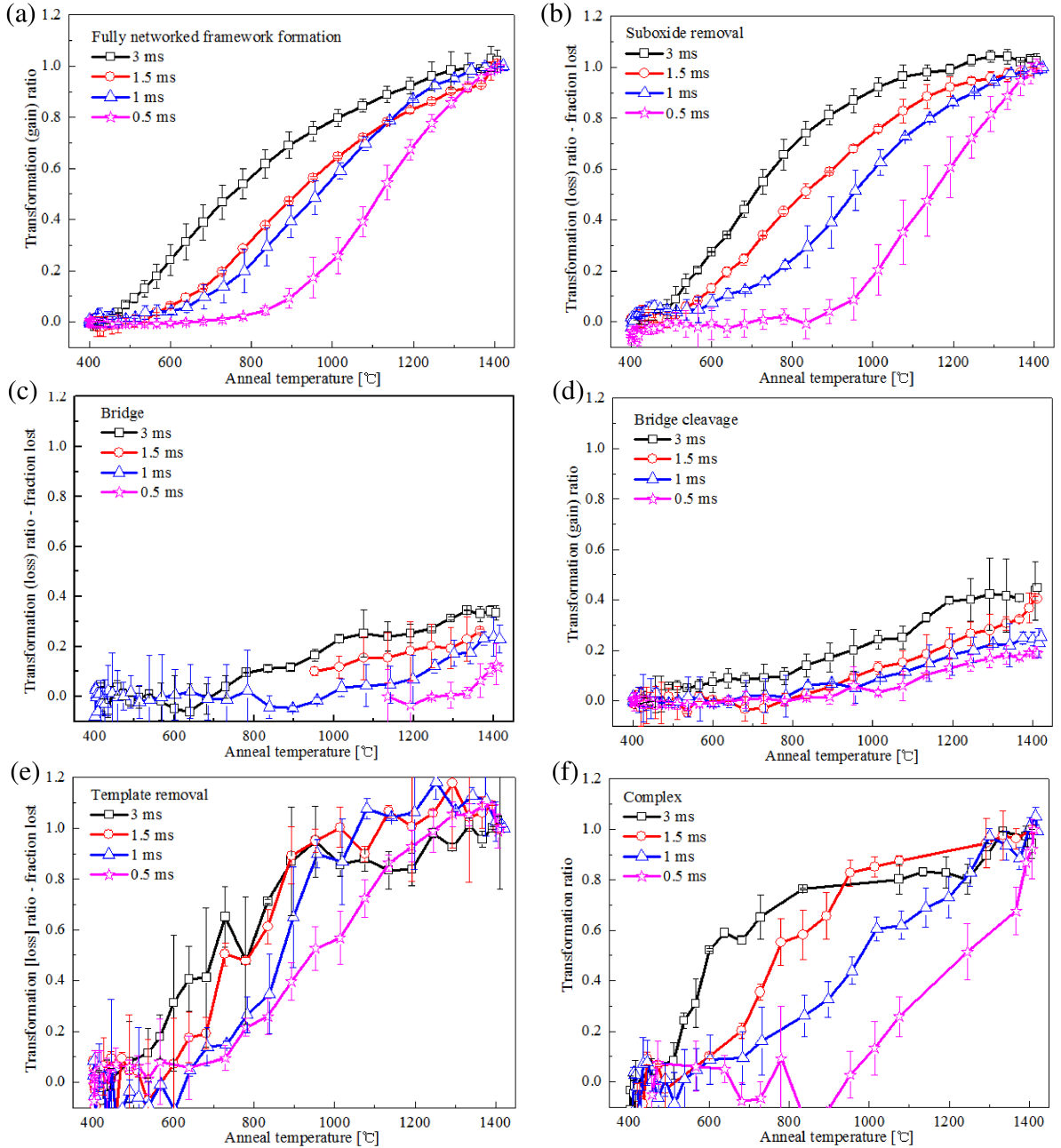


**Figure 3:** Structural transformation dynamics as a function of LSA temperature at different dwells. (a) Fully networked framework formation, (b) sub-oxide removal, (c) bridge ( $\text{Si-C}_2\text{H}_4\text{-Si}$ ), (d) bridge cleavage ( $\text{Si-C}_2\text{H}_5$ ), (e) template removal ( $\text{CH}_x$ ), and (f) complex [ $\text{CH}_3^+$ ].

confirming the limited loss of bridges for short dwells. At the 0.5 ms dwell, bridge cleavage is minimal until  $\sim 1000^\circ\text{C}$ , while at 3 ms dwell the significant loss is observed even by  $\sim 800^\circ\text{C}$ . While the onset of loss occurs earlier for long dwells, the total loss is only 20% for 0.5 ms or 40% for 3 ms dwells at the highest LSA heating temperature.

The template removal was quantified using the [ $\text{CH}_x$ ] FTIR peak at  $2860\text{--}2920\text{ cm}^{-1}$  (Figure 3e); as other chemical entities also would contribute to this peak, we assume full conversion occurs at the highest temperatures as evidenced by the saturation of this peak above  $1000^\circ\text{C}$  (Figure S4c). The template removal depends primarily on the peak temperature with only weak dependence on the dwell. By  $1000^\circ\text{C}$ , nearly all the tem-

plates are lost for the 1–3 ms annealed samples, and  $> 60\%$  for the 0.5 ms sample.

The  $[\text{CH}_3+]$  organic complexes FTIR peak (Figure 3f) is also related to the template loss but exhibits slightly different behaviors. This peak shows much stronger dwell dependence and mimics more of the network-forming kinetics. This suggests the signal arises from multiple entities including the template, organic  $\text{SiO}_x\text{C}_y$  sub-oxide, and carbon bridges.

## 2.2 Activation energies

Taking advantage of an extended temperature range for each dwell, activation energies were extracted from Arrhenius plots of the six structural transformations as shown in **Figure 4**. Data were fit to the Arrhenius equation,

$$\text{Rate} = C e^{-E_a / RT},$$

where  $E_a$  is the activation enthalpy,  $T$  is the LSA heating peak temperature,  $R$  is the gas constant (8.314 J/mol), and  $C$  is a constant pre-factor. Activation energies were calculated from the slopes of the log rate versus  $1/T$ , with slopes essentially independent of the dwell. **Table 2** summarizes these critical activation energies.

We find that template removal and full-network formation require the highest activation energies (50–62 kJ/mol), while removal of sub-oxide and complex  $[\text{CH}_3+]$  show the smallest activation energies (30–46 kJ/mol). The bridge-cleavage indicators ( $\text{Si-CH}_2\text{CH}_3$  and  $\text{Si-CH}_2\text{-CH}_2\text{-Si}$ ) exhibit an intermediate range of activation energies (45–51 kJ/mol). This suggests that removal of large organic molecules and relaxation of the inorganic framework will be more difficult to kinetically activate than the local relaxation of small organic structures.

With increasing temperature and correspondingly shorter times, processes with high activation energies (template removal and network formation) will be kinetically accelerated more rapidly than low activation processes (bridge cleavage and sub-oxide removal). This provides a kinetic pathway to optimize overall film development during thermal annealing.

**Table 2:** Summary of activation energies ( $E_a$ ) for different structural transformations.

Structural transformation	Template removal	Fully networked	Bridge cleavage	Bridge	Sub-oxide removal	Complex $[\text{CH}_3+]$
$E_a$ [kJ/mol]	$58 \pm 4$	$53 \pm 2.5$	$49 \pm 1.8$	$47 \pm 2.4$	$44 \pm 1.6$	$32 \pm 1.8$

## 2.3 Effective local heating time

In contrast to isothermal anneals, LSA temperatures vary rapidly with time and are characterized by a dwell time ( $\tau_{\text{dwell}}$ ). Using the determined activation energies, the ef-



fective time at the peak temperature ( $T_{\max}$ ) is given by

$$t_{\text{eff}} = \int \exp \left\{ -\frac{E_a}{k} \left[ \frac{1}{T(t)} - \frac{1}{T_{\max}} \right] \right\} dt,$$

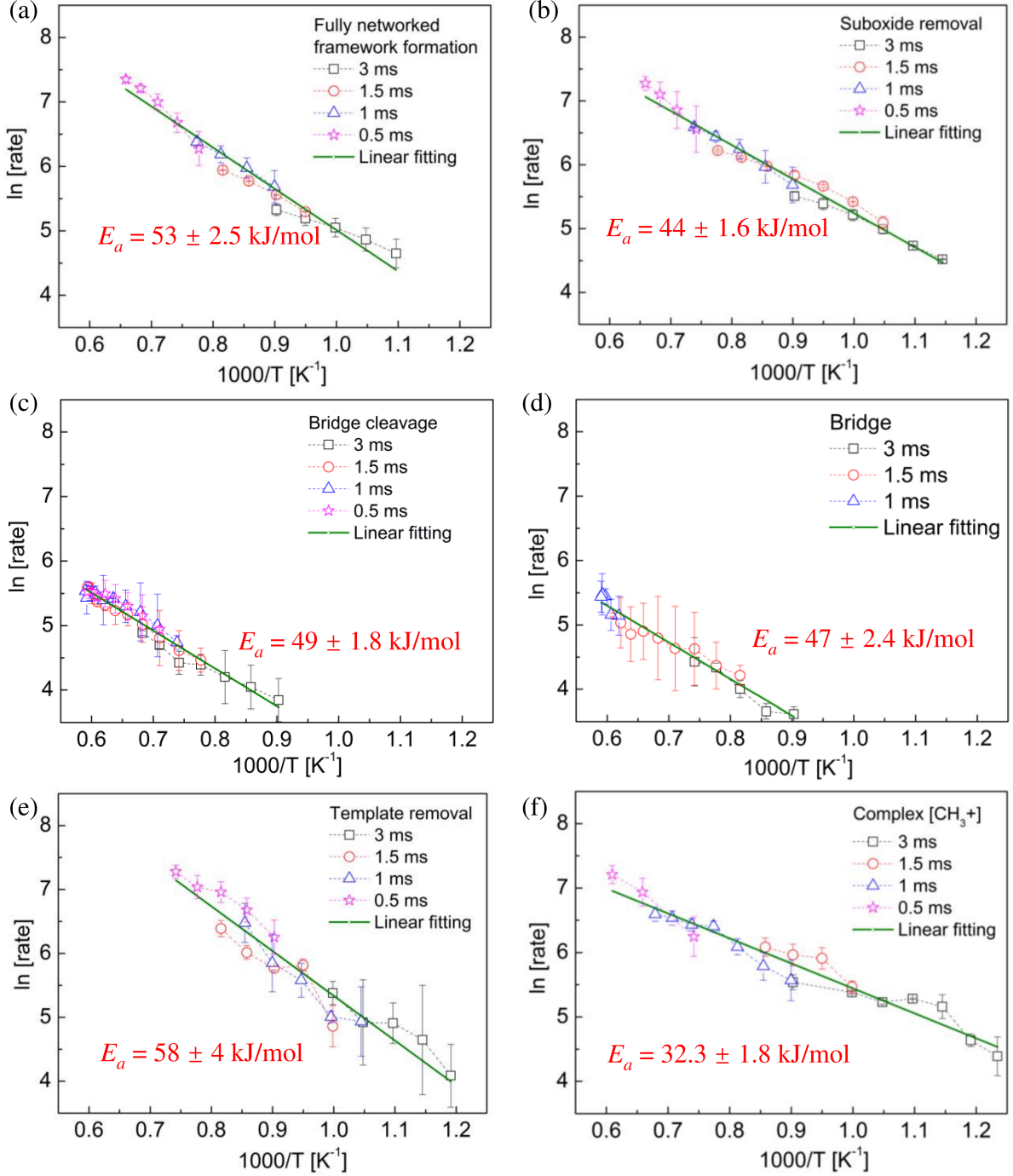


**Figure 4:** Arrhenius plots and activation energies for the structural transformation. (a) Fully networked framework formation, (b) sub-oxide removal, (c) bridge cleavage via  $\text{Si-CH}_2\text{CH}_3$  formation, (d) bridge cleavage via loss of  $\text{Si-CH}_2\text{CH}_2\text{-Si}$ , (e) template (porogen) removal ( $\text{CH}_x$ ), and (f) organic complex loss  $[\text{CH}_3+]$ . Datasets for bridge cleavage and bridge motifs are taken at a transformation range from 10% to the highest transformation limit; all other datasets are taken at a fixed transformation range from 25% to 75%.

where  $E_a$  is the activation energy,  $k$  is the Boltzmann constant, and  $T(t)$  is the time-dependent temperature. The time dependence  $T(t)$  was determined from heat-flow simulations using CLASP [46]. As shown in **Figure 5a**, different laser dwells result in a distinctive variation in effective heating duration. For a 3 ms dwell, the effective time is  $\sim 40$  ms, while 0.5 ms dwell samples experienced  $\sim 1.5$  ms effective heating, with small variations due to the different activation energies. The increase in  $t_{\text{eff}} / \tau_{\text{dwell}}$  with increasing dwell arises from the transition from a thermally thick substrate (fast quench) to a thermally thin substrate (slow quench).

## 2.4 Stretched exponential relaxation

While the bridge-cleavage activation energy is not significantly higher than that for the template removal (Table 2), the structural dynamic data (Figure 3c,d) demonstrates that bridge cleavage is substantially minimized under sub-millisecond heating. Understanding this behavior requires determining the fundamental processes that control structural transformations in PMOs and their detailed kinetic rates.

Structural transformations require a continuous supply of reactive species that diffuse

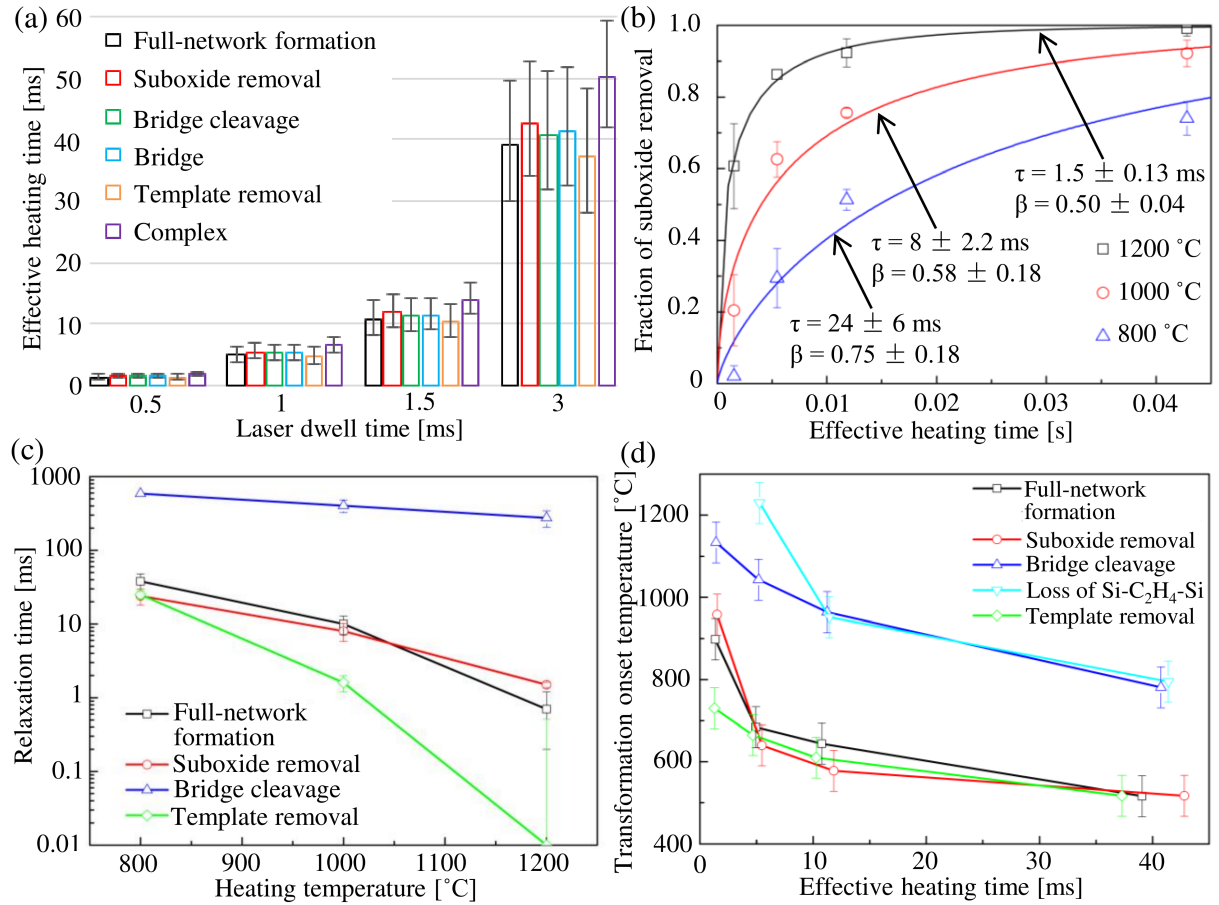


**Figure 5:** Kinetic analysis of structural transformation. (a) Effective local heating time for various laser dwells and structural transformations at  $T_{\text{max}} \simeq 1400^\circ\text{C}$ . (b) Example of fitting the stretched exponential for sub-oxide removal. (c) Relaxation time for transformations as a function of temperature. (d) Onset temperature for 10% transformations as a function of heating duration.

from the bulk surface, or that are generated within the film. For disordered transformations with a range of activation energies, the stretched exponential is commonly used to model transformation kinetics [47, 48, 49, 50, 51]. The PMO structure contains both ordered and periodic features (pores separated by Si-O based wall as shown in Figure 1), with carbon-bridge motifs randomly inserted in the networked wall [6, 8, 9, 10]. This complex system is expected to follow a diffusion-controlled stretched exponential expression featuring random-distributed, time-dependent diffusion.

To support this exponential relaxation mechanism, we propose possible reaction and diffusion routes in PMOs (see details in Supplementary Information). Diffusive species considered include water ( $\text{H}_2\text{O}$ ), hydrogen ( $\text{H}_2$ ), protons ( $\text{H}_0$ ), oxygen ( $\text{O}_2$ ), and organic molecules such as  $\text{CH}_2$  and  $\text{C}_2\text{H}_5\text{OH}$ . To estimate their behaviors in the local PMO environment (Figure S5a,b), we summarize in Table S1 [52, 53, 54, 55, 56, 57, 58, 59] diffusion parameters (activation energy, diffusion coefficient, diffusion length, and reaction mechanism) of these species in amorphous  $\text{SiO}_x$ , amorphous  $\text{SiC}$ , and PDMS (a silicon-based organic polymer). Based on these values and our measured values, we hypothesize that  $\text{H}_2\text{O}$ , generated from crosslinking (Figure S5c), is likely the limiting diffusion species in the PMO film. At temperatures studied,  $\text{H}_2\text{O}$  diffusion lengths are comparable to the reported 4.2-nm-thick networked wall of PMOs [22], making  $\text{H}_2\text{O}$ -assisted reactions challenging compared to other species with large diffusion lengths. We further propose that  $\text{H}_2\text{O}$ -assisted reactions inducing template removal and pore generation [60] (Figure S5d), sub-oxide removal through typical hydrolysis (Figure S5e), and bridge cleavage (Figure S5f) are limiting steps. However, this paper focuses on the processing kinetics, and detailed chemical reaction routes will require further investigation.

Transformation dynamics were fit by a stretched exponential (Figure 5b)

$$X = 1 - \exp \left[ - \left( \frac{t}{\tau} \right)^\beta \right],$$

where  $X$  is the transformation ratio,  $t$  is the time,  $\tau$  is a characteristic time constant (required relaxation time), and  $\beta$  is an index that reflects coupling of relaxation processes. Details of fitting for different motifs are included in Figure S6, together with the summarized parameters in Table S2 and S3.

The relaxation time constants for structural transformations are presented in Figure 5c as a function of the peak temperature. The time to induce bridge cleavage (200–600 ms) is significantly higher than that for framework formation, sub-oxide removal, and template removal (1–50 ms). For example, at 1200 °C, the relaxation time for bridge cleavage is  $\sim 300$  ms, while for framework formation and template removal, it is only  $\sim 1$  ms. This large difference in relaxation times enables the manipulation of different structural modifications using the time and temperature trade-off. This behavior reflects on the essentially higher onset temperatures for bridge cleavage than other transformations (Figure 5d).

**Table 3:** Comparison of the ratio of the effective heating time to the structural relaxation time at 1200 °C for 0.5 ms and 3 ms dwells.

Laser dwell	Bridge cleavage	Sub-oxide removal	Fully networked	Template removal
0.5 ms	$0.005 \pm 0.3$	$1 \pm 0.22$	$2 \pm 0.7$	$> 30$
3 ms	$0.15 \pm 0.3$	$29 \pm 0.21$	$56 \pm 0.7$	$> 800$

**Table 3** compares the ratio of effective heating at 1200 °C for 0.5 ms and 3 ms dwells to the relaxation time constant. Even at 1200 °C for 3 ms, there is insufficient time to significantly impact the bridge cleavage ( $t_{\text{eff}} / \tau_{\text{relax}} = 0.15 \pm 0.3$ ), while for 0.5 ms there is already sufficient time for complete network formation and template/sub-oxide removal.

## 2.5 Transformation diagram and heat treatment design

In order to facilitate PMO applications, the structural transformation diagram with critical heating temperature versus time is shown in **Figure 6**. In these diagrams, the green curve represents the maximum temperature that can be tolerated with minimal loss ( $< 10\%$ ) of the bridge motif. For each motif, except the bridge, the onset ( $< 10\%$ ), completion ( $> 90\%$ ), and 50% transformation curves are shown. For the bridge cleavage, the 20% and 40% transformation curves are shown with an estimate for the temperature that would be required to achieve 50% transformation. To avoid significant loss of bridge structures, the suboxide-to-network conversion is limited to  $\sim 50\%$  while the template conversion is nearly completed. At the other extreme, the purple curves show the minimum temperature required as a function of heating time to fully convert the network. Loss of bridge motif is minimized by the shortest heating times with less than 20% loss for  $t_{\text{heat}} = 1$  ms.

## 3 Conclusion

In summary, the annealing kinetics of bridged PMOs were investigated as a function of LSA peak temperatures (400–1400 °C) and dwells (0.5–3 ms). We established the transformation dynamics of bridge cleavage, framework formation, and template removal, with activation energies of  $58 \pm 4$  kJ/mol for template removal,  $53 \pm 2.5$  for formation of the full network,  $48 \pm 2$  for bridge loss, and  $44 \pm 1.6$  for removal of sub-oxide structures.

While the activation energies for the various processes are similar, the kinetics vary significantly quantified by a relaxation time. At 1200 °C, the relaxation times are 300 ms for bridge cleavage but only  $\approx 1$  ms for framework formation and template removal. This large difference in relaxation times allows network formation to be completed while the bridge cleavage is minimized under heating at sufficiently high temperature and short times.

In applying this finding to heat treatment design, a time-temperature-transformation

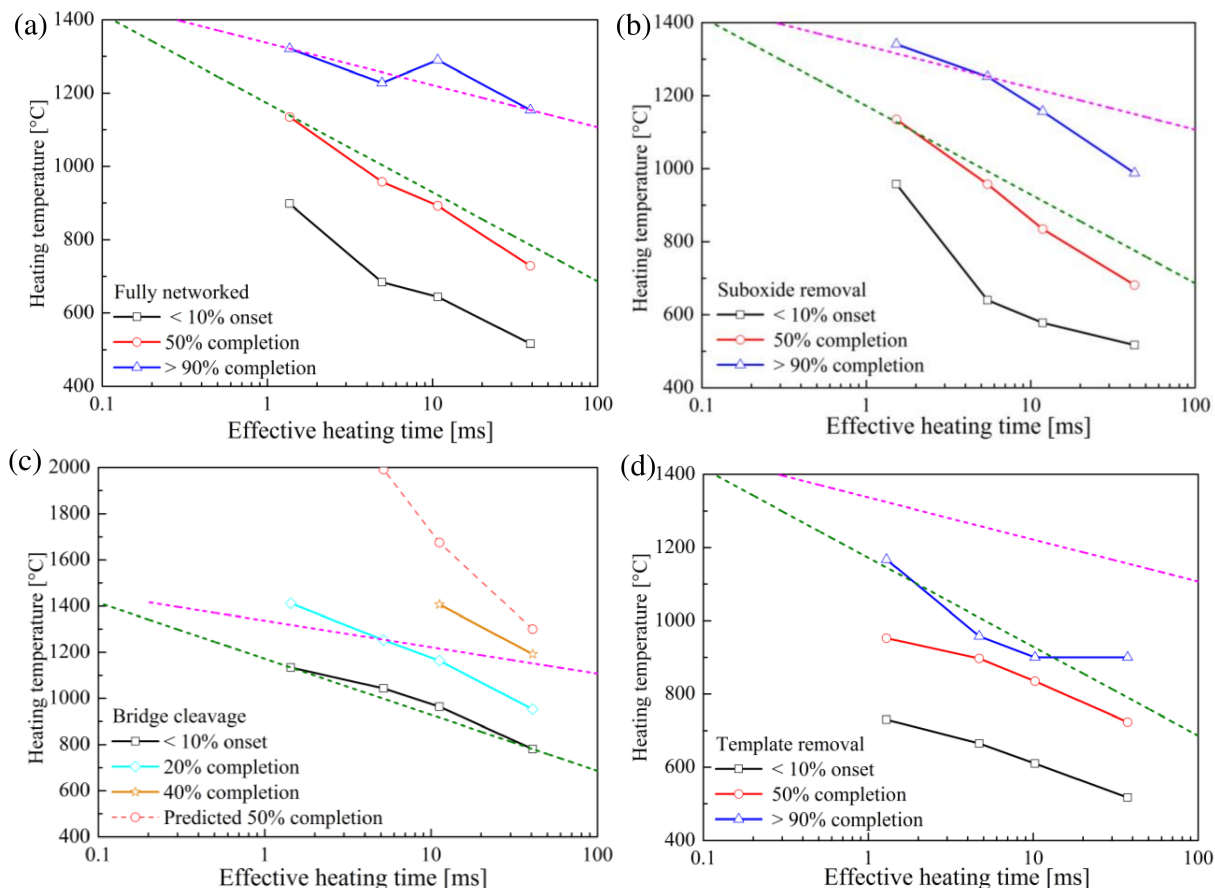


**Figure 6:** Structural transformation diagram showing critical points during different transformation stages. (a) framework formation, (b) sub-oxide removal, (c) bridge cleavage (Si-C<sub>2</sub>H<sub>5</sub>), (d) template removal (CH<sub>x</sub>). The green dash line represents the maximum temperature at each dwell that can be tolerated with minimized loss of the bridge motif (set by 6c). The purple dash line represents the minimum temperature at each dwell that fully transforms the required framework and template (set by 6a).

diagram is developed. Effects of porosity and reaction routes (see Supplementary Information) could be further studied using this same methodology. The control of framework and pore formation without bridge cleavage could enable new synthesis and post processing, and facilitate the transition of PMO-class materials to broad applications.

## 4 Experimental Section

### *Sol-gel PMO-film synthesis:*

1,2-Bis(triethoxysilyl)ethane (BTEE, 96%), Brij-76, and 2-methoxy-1-propanol (PMOH, > 99.5%) were purchased from Sigma-Aldrich and used as received without further purification.

Ethyl-bridged periodic mesoporous organosilicas (PMOs) were synthesized in PMOH solution at room temperature through a template-directed sol-gel process. The precursor BTEE and template (porogen) Brij-76 were diluted separately in PMOH to 25 wt% concentration. The template was added to the BTEE solution at 9–21.5 wt% ratios, and

then 0.61 mL nitric acid (1 M) was added per gram of BTEE. The solution was aged for 15 minutes.

PMO thin films were prepared by spin-coating on nominally undoped bare Si wafers at 2000 RPM for 90 seconds. Films were immediately baked at 85 °C for 2 minutes on a hotplate, followed by pre-cure baking at 400 °C for 1 hour in a vacuum box oven (Yield Engineering Systems, 450PB). This pre-cure allowed the initialization of sol-gel reactions and provided an initial porous environment with the necessary frameworks for the high-temperature LSA investigations. After the pre-cure bake, films were  $\sim 300$  nm thick.

The sol-gel hydrolysis and condensation reactions of precursors and templates (porogen) are given in Figure S10, and their intermediate structures, as determined by FTIR, are shown in Figure S11. Figure S12 shows the ideal chemical structure of a resulting film with intrinsic carbon bridges embedded in the Si-O network.

#### *Characterization:*

Chemical structure changes were determined using transmission FTIR (Fourier-transform infrared spectroscopy, Bruker Hyperion) and XPS (X-ray photoelectron spectroscopy). In order to achieve spatially resolved characterization, FTIR measurements were obtained with a 20  $\mu\text{m}$  aperture scanned across the  $\sim 700$   $\mu\text{m}$  laser-annealed lines with spectra every 25  $\mu\text{m}$ . The FTIR spectra were fit to nine Gaussian peaks (in four sets): precursor peaks of Si-OH at 900  $\text{cm}^{-1}$  and Si-OCH<sub>2</sub>CH<sub>3</sub> at 930  $\text{cm}^{-1}$ ; Si-O framework peaks of sub-oxide at 1023–1035  $\text{cm}^{-1}$ , fully networked Si-O framework at 1065–1072  $\text{cm}^{-1}$ , and ladder structure at 1105  $\text{cm}^{-1}$ ; carbon-bridge related peaks of Si-CH<sub>2</sub>-CH<sub>2</sub>-Si at 1150–1162  $\text{cm}^{-1}$  and Si-CH<sub>2</sub>CH<sub>3</sub> (bridge cleavage) at 1220  $\text{cm}^{-1}$ ; and template (porogen) peaks of complex CH<sub>x</sub> at 2860–2920  $\text{cm}^{-1}$  and CH<sub>3</sub>+ at 1272–1275  $\text{cm}^{-1}$ . Details of the fitting procedure have been published previously [40], with detailed analyses of the sol-gel reactions after deposition and pre-cure given in the Supplementary Information.

#### *Laser spike annealing (LSA):*

Following pre-cure, films were annealed to high temperatures using the lateral gradient (single-stripe) LSA (lgLSA) technique [45]. A 120 W CO<sub>2</sub> laser ( $\lambda = 10.6$   $\mu\text{m}$ ) was focused to a line-shape beam ( $\sim 95$   $\mu\text{m} \times \sim 700$   $\mu\text{m}$ ) and scanned across films/substrates mounted on a 400 °C pre-heated vacuum chuck. The lateral intensity of the laser was intentionally near Gaussian to establish a lateral temperature profile across laser scans. Dwell time, defined as the laser FWHM in the scan direction divided by the scan velocity, was varied between 0.5 and 3 ms. Peak temperature at the center of each stripe was adjusted by the incident laser power using an optical attenuator, with peak temperatures for 400 °C (hot stage) to  $\sim 1400$  °C (Si melt). Temperatures were calibrated using Si and Au melt coupled with CLASP heat flow simulations [46].

## **Supporting Information**

Supporting Information is in another file, including FTIR and XPS analyses on sol-gel samples, details on structural dynamics and stretched exponential fitting; discussions on the effects of porosity and on possible reaction routes in PMO annealing.

### Acknowledgements

The work was supported by the Semiconductor Research Corporation (SRC), Global-Foundries, and Intel. This work was performed in part at the Cornell NanoScale Facility, an NNCI member supported by NSF Grant NNCI-2025233, and made use of the Cornell Center for Materials Research Shared Facilities which are supported through the NSF MRSEC program (DMR-1719875). Z.S. acknowledges Dr. Y. Sun and Dr. D. Zhang for experimental assistance.

### Author Contributions

Z.S. performed the experiments, characterizations, and analyses. A.C. assisted with laser spike annealing and thermal analysis. M.O.T. supervised the work and analyzed the data. Z.S. and M.O.T. wrote the manuscript.

### Conflicts of Interest

The authors declare no competing financial interests.

### Data Availability Statement

Data are available by contacting the corresponding author.

## References

- <sup>1</sup> M. E. Davis, *Nature* **2002**, *417* 813.
- <sup>2</sup> C. T. Kresge, M. E. Leonowicz, W. J. Roth, J. C. Vartuli, J. S. Beck, *Nature* **1992**, *359* 710.
- <sup>3</sup> T. Asefa, M. J. MacLachlan, N. Coombs, G. A. Ozin, *Nature* **1999**, *402* 867.
- <sup>4</sup> B. J. Melde, B. T. Holland, C. F. Blanford, A. Stein, *Chem. Mater.* **1999**, *11* 3302.
- <sup>5</sup> S. Inagaki, S. Guan, Y. Fukushima, T. Ohsuna, O. Terasaki, *J. Am. Chem. Soc.* **1999**, *121* 9611.
- <sup>6</sup> P. Van Der Voort, D. Esquivel, E. De Canck, F. Goethals, I. Van Driessche, F. J. Romero-Salguero, *Chem. Soc. Rev.* **2013**, *42* 3913.
- <sup>7</sup> M. Jaroniec, *Nature* **2006**, *442* 638.
- <sup>8</sup> S. S. Park, M. S. Moorthy, C. S. Ha, *NPG Asia Mater.* **2014**, *6* e96.
- <sup>9</sup> B. D. Hatton, K. Landskron, W. J. Hunks, M. R. Bennett, D. Shukaris, D. D. Perovic, G. A. Ozin, *Mater. Today* **2006**, *9* 22.
- <sup>10</sup> F. Hoffmann, M. Cornelius, J. Morell, M. Froba, *Angew. Chem. Int. Ed.* **2006**, *45* 3216.

- <sup>11</sup> D. A. Loy, K. J. Shea, *Chem. Rev.* **1995**, *95* 1431.
- <sup>12</sup> R. J. P. Corriu, D. Leclercq, *Angew. Chem. Int. Ed.* **1996**, *35* 1420.
- <sup>13</sup> B. Hatton, K. Landskron, W. Whitnall, D. Perovic, G. A. Ozin, *Acc. Chem. Res.* **2005**, *38* 305.
- <sup>14</sup> T. Asefa, M. J. MacLachlan, H. Grondey, N. Coombs, G. A. Ozin, *Angew. Chem. Int. Ed.* **2000**, *39* 1808.
- <sup>15</sup> S. Guan, S. Inagaki, T. Ohsuna, O. Terasaki, *J. Am. Chem. Soc.* **2000**, *122* 5660.
- <sup>16</sup> M. Kruk, M. Jaroniec, S. Guan, S. Inagaki, *J. Phys. Chem. B* **2001**, *105* 681.
- <sup>17</sup> M. P. Kapoor, S. Inagaki, *Chem. Mater.* **2002**, *14* 3509.
- <sup>18</sup> A. Sayari, Y. Yang, *Chem. Commun.* **2002**, 2582.
- <sup>19</sup> O. Muth, C. Schellbach, M. Froba, *Chem. Commun.* **2001**, 2032.
- <sup>20</sup> H. Zhu, D. J. Jones, J. Zajac, J. Roziere, R. Dutartre, *Chem. Commun.* **2001**, 2568.
- <sup>21</sup> Z. Zhou, R. N. K. Taylor, S. Kullmann, H. Bao, M. Hartmann, *Adv. Mater.* **2011**, *23* 2627.
- <sup>22</sup> E. Cho, K. Char, *Chem. Mater.* **2004**, *16* 270.
- <sup>23</sup> D. Esquivel, C. Jimenez-Sanchidrian, F. J. Romero-Salguero, *Mater. Lett.* **2011**, *65* 1460.
- <sup>24</sup> W. Wang, S. Xie, W. Zhou, A. Sayari, *Chem. Mater.* **2004**, *16* 1756.
- <sup>25</sup> K. Nakajima, I. Tomita, M. Hara, S. Hayashi, K. Domen, J. N. Kondo, *J. Mater. Chem.* **2005**, *15* 2362.
- <sup>26</sup> S. Inagaki, G. S., T. Ohsuna, O. Terasaki, *Nature* **2002**, *416* 304.
- <sup>27</sup> M. P. Kapoor, Q. Yang, S. Inagaki, *Chem. Mater.* **2004**, *16* 1209.
- <sup>28</sup> Y. Goto, S. Inagaki, *Chem. Comm.* **2002**, 2410.
- <sup>29</sup> J. Morell, G. Wolter, M. Froba, *Chem. Mater.* **2005**, *17* 804.
- <sup>30</sup> E. Cho, J. Park, M. Jaroniec, *J. Phys. Chem. C* **2013**, *117* 21441.
- <sup>31</sup> K. Landskron, B. D. Hatton, D. D. Perovic, G. A. Ozin, *Science* **2003**, *302* 266.
- <sup>32</sup> M. C. Burleigh, S. Jayasundera, M. S. Spector, C. W. Thomas, M. A. Markowitz, B. P. Gaber, *Chem. Mater.* **2004**, *16* 3.
- <sup>33</sup> E. Cho, D. Kim, M. Jaroniec, *Langmuir* **2007**, *23* 11844.
- <sup>34</sup> M. Burleigh, M. A. Markowitz, M. S. Spector, B. P. Gaber, *J. Phys. Chem. B* **2001**, *105* 9935.



- <sup>35</sup> Y. Xia, W. Wang, R. Mokaya, *J. Am. Chem. Soc.* **2005**, *127* 790.
- <sup>36</sup> W. Zhang, B. Daly, J. O’Callaghan, L. Zhang, J. Shi, C. Li, M. A. Morris, J. D. Holmes, *Chem. Mater.* **2005**, *17* 6407.
- <sup>37</sup> P. Yang, D. Zhao, D. I. Margolese, B. F. Chmelka, G. D. Stucky, *Chem. Mater.* **1999**, *11* 2813.
- <sup>38</sup> M. J. MacLachlan, N. Coombs, G. A. Ozin, *Nature* **1999**, *397* 681.
- <sup>39</sup> H. Fan, Y. Lu, A. Stump, S. T. Reed, T. Baer, R. Schunk, V. Perez-Luna, G. P. Lopez, C. J. Brinker, *Nature* **2000**, *405* 56.
- <sup>40</sup> Z. Sun, R. T. Bell, M. O. Thompson, *ACS Appl. Electron. Mater.* **2019**, *1* 1243.
- <sup>41</sup> A. Sayari, S. Hamoudi, *Chem. Mater.* **2001**, *13* 3151.
- <sup>42</sup> C. Yoshina-Ishii, T. Asefa, N. Coombs, M. J. MacLachlan, G. A. Ozin, *Chem. Commun.* **1999**, 2539.
- <sup>43</sup> W. Volksen, R. D. Miller, G. Dubois, *Chem. Rev.* **2010**, *110* 56.
- <sup>44</sup> D. Esquivel, E. D. Canck, C. Jimenez-Sanchidrian, P. Van Der Voort, F. J. Romero-Salguero, *J. Mater. Chem.* **2011**, *21* 10990.
- <sup>45</sup> R. T. Bell, A. G. Jacobs, V. C. Sorg, B. Jung, M. O. Hill, B. E. Trembl, M. O. Thompson, *ACS Comb. Sci.* **2016**, *18* 548.
- <sup>46</sup> K. Iyengar, B. Jung, M. Willemann, P. Clancy, M. O. Thompson, *Appl. Phys. Lett.* **2012**, *100* 211915.
- <sup>47</sup> J. C. Phillips, *Rep. Prog. Phys.* **1996**, *59* 1133.
- <sup>48</sup> J. Kakalios, R. A. Street, W. B. Jackson, *Phys. Rev. Lett.* **1987**, *59* 1037.
- <sup>49</sup> D. C. Johnston, *Phys. Rev. B* **2006**, *74* 184430.
- <sup>50</sup> B. Sturman, E. Podivilov, M. Gorkunov, *Phys. Rev. Lett.* **2003**, *91* 176602.
- <sup>51</sup> W. Primak, *Phys. Rev.* **1955**, *100* 1677.
- <sup>52</sup> D. L. Griscom, *J. Appl. Phys.* **1985**, *58* 2524.
- <sup>53</sup> B. Tuttle, *Phys. Rev. B* **2000**, *61* 4417.
- <sup>54</sup> T. Bakos, S. N. Rashkeev, S. T. Pantelides, *Phys. Rev. Lett.* **2002**, *88* 055508.
- <sup>55</sup> R. A. Causey, J. D. Fowler, C. Ravanbakht, T. S. Elleman, K. Verghese, *J. Am. Ceram. Soc.* **1978**, *6* 221.
- <sup>56</sup> H. He, M. Deshpande, R. Brown, R. Pandey, U. Pernisz, *J. Appl. Phys.* **2005**, *98* 023519.

<sup>57</sup> M. D. Ventra, S. T. Pantelides, *J. Electron. Mater.* **2000**, *29* 353.

<sup>58</sup> D. Hofmann, L. Fritz, J. Ulbrich, C. Schepers, M. Bohning, *Macromol. Theory Simul.* **2000**, *9* 293.

<sup>59</sup> J. A. Barrie, B. Platt, *Polym.* **1963**, *4* 303.

<sup>60</sup> D. D. Burkey, K. K. Gleason, *J. Vac. Sci. Technol.* **2004**, *22* 61.